FULL PAPER

CrossMark

High Frequency Analyzer (HFA) of Plasma Wave Experiment (PWE) onboard the Arase spacecraft

Atsushi Kumamoto[1*] , Fuminori Tsuchiya[1], Yoshiya Kasahara[2], Yasumasa Kasaba[1], Hirotsugu Kojima[3], Satoshi Yagitani[2], Keigo Ishisaka[4], Tomohiko Imachi[2], Mitsunori Ozaki[2], Shoya Matsuda[5], Masafumi Shoji[5], Aayako Matsuoka[6], Yuto Katoh[1], Yoshizumi Miyoshi[5] and Takahiro Obara[1]

Abstract

The High Frequency Analyzer (HFA) is a subsystem of the Plasma Wave Experiment onboard the Arase (ERG) spacecraft. The main purposes of the HFA include (1) determining the electron number density around the spacecraft from observations of upper hybrid resonance (UHR) waves, (2) measuring the electromagnetic field component of whistler-mode chorus in a frequency range above 20 kHz, and (3) observing radio and plasma waves excited in the storm-time magnetosphere. Two components of AC electric fields detected by Wire Probe Antenna and one component of AC magnetic fields detected by Magnetic Search Coils are fed to the HFA. By applying analog and digital signal processing in the HFA, the spectrograms of two electric fields (EE mode) or one electric field and one magnetic field (EB mode) in a frequency range from 10 kHz to 10 MHz are obtained at an interval of 8 s. For the observation of plasmapause, the HFA can also be operated in PP (plasmapause) mode, in which spectrograms of one electric field component below 1 MHz are obtained at an interval of 1 s. In the initial HFA operations from January to July, 2017, the following results are obtained: (1) UHR waves, auroral kilometric radiation (AKR), whistler-mode chorus, electrostatic electron cyclotron harmonic waves, and nonthermal terrestrial continuum radiation were observed by the HFA in geomagnetically quiet and disturbed conditions. (2) In the test operations of the polarization observations on June 10, 2017, the fundamental R-X and L-O mode AKR and the second-harmonic R-X mode AKR from different sources in the northern polar region were observed. (3) The semiautomatic UHR frequency identification by the computer and a human operator was applied to the HFA spectrograms. In the identification by the computer, we used an algorithm for narrowing down the candidates of UHR frequency by checking intensity and bandwidth. Then, the identified UHR frequency by the computer was checked and corrected if needed by the human operator. Electron number density derived from the determined UHR frequency will be useful for the investigation of the storm-time evolution of the plasmasphere and topside ionosphere.

Keywords: The Arase (ERG) spacecraft, Plasma Wave Experiment (PWE), High Frequency Analyzer (HFA), Upper hybrid resonance (UHR) wave, Auroral kilometric radiation (AKR), Whistler-mode chorus, Electrostatic electron cyclotron harmonic (ESCH) wave, Nonthermal terrestrial continuum (NTC) radiation, Electron number density, Plasmasphere

*Correspondence: kumamoto@stpp.gp.tohoku.ac.jp
[1] Tohoku University, 6-3, Aoba, Aramaki, Aoba, Sendai 980-8578, Japan
Full list of author information is available at the end of the article

Kumamoto *et al. Earth, Planets and Space* (2018) 70:82

Page 2 of 14

Introduction

The High Frequency Analyzer (HFA) is a subsystem of the Plasma Wave Experiment (PWE) onboard the Arase (ERG, Exploration of energization and Radiation in Geospace) spacecraft for the observation of radio and plasma waves in a frequency range from 10 kHz to 10 MHz. The Arase spacecraft was launched on December 20, 2016. The inclination of the Arase satellite is 31°, and the altitudes of the apogee and perigee are ∼ 32,000 and 460 km, respectively. The orbital period is approximately 570 min. The purpose of the mission is to explore the plasma dynamics of Earth's radiation belt using electric and magnetic field instruments covering a wide frequency range and electron and ion detectors over a wide energy range (Miyoshi et al. 2012; Miyoshi et al. in review). A new instrument, S-WPIA (Software-Type Wave–Particle Interaction Analyzer), was installed on the satellite to perform direct measurement of the energy exchange between plasma waves and particles (Katoh et al. 2018; Hikishima et al. 2018). The observations of DC electric fields and AC electromagnetic fields of radio and plasma waves are performed by the PWE (Kasahara et al. 2018b), which consists of four sets of Wire Probe Antenna (WPT) (Kasaba et al. 2017), three-axial Magnetic Search Coils (MSC) (Ozaki et al. 2018), and a DC Electric Field Detector (EFD) (Kasaba et al. 2017), Wave Form Capture and Onboard Frequency Analyzer (WFC/OFA) (Kasahara et al. 2018b; Matsuda et al. 2018), and HFA.

Under the Arase mission, the HFA is expected to perform the following: (1) Determine the electron number density around the spacecraft based on observations of upper hybrid resonance (UHR) waves. Previous studies suggested that the whistler-mode chorus emission just outside of the plasmapause contributed to the recovery of the radiation belt electrons in the recovery phase of geomagnetic storms (e.g., Miyoshi et al. 2003). Knowing the location of the plasmapause is of fundamental importance for understanding the distribution of the plasma waves associated with the loss and generation of the relativistic electrons. In addition, electron number density is a key parameter in discussion of resonance conditions between the plasma waves and electrons that generate the plasma waves. The energy range of the electrons estimated from the resonance conditions will be useful in onboard analyses of wave–particle interactions by S-WPIA. (2) Measure the electromagnetic field component of the whistler-mode chorus in a frequency range above 20 kHz up to 100 kHz. The whistler-mode chorus is one of the most important targets of the Arase mission. Throughout most of the orbit, the chorus can be observed by WFC/OFA, which covers a frequency range below 20 kHz. However, around the perigee where the electron cyclotron frequency is higher than 20 kHz,

the frequency range of the chorus cannot be covered by WFC/OFA. Therefore, the HFA was designed to measure not only the AC electric fields, which are enough for observation of UHR, but also AC magnetic fields above 20 kHz. (3) Detect radio and plasma waves excited by wave–particle interactions and mode conversion processes in storm-time magnetosphere. The frequency of radio and plasma waves depends on the electron cyclotron frequency and the plasma frequency in their source regions. The electron cyclotron frequency and plasma frequency in the inner magnetosphere and upper ionosphere mostly fall in the HFA range of 10 kHz to 10 MHz.

In order to achieve the requirements mentioned above, the HFA was designed based on the heritage of radio and plasma wave receivers installed on Japanese spacecraft such as Jikiken (EXOS-B) (Oya et al. 1981), Ohzora (EXOS-C) (Oya et al. 1985), Akebono (EXOS-D) (Oya et al. 1990), Nozomi (Planet-B) (Ono et al. 1998), and Kaguya (SELENE; Selenological and Engineering Explorer) (Ono et al. 2008, 2010). To determine some specifications such as frequency resolution and dynamic range, we considered the past analyses of datasets obtained by Akebono/PWS (Plasma Waves and Sounder Experiment). The hardware design of the HFA was based on that of the NPW-W (Natural Plasma Wave-Waveform) receiver of Kaguya/LRS (Lunar Radar Sounder).

This paper is an initial report of the details regarding the HFA instrument and some of the results obtained in the initial HFA operation. In "Instruments" section, the detailed design of the hardware, onboard digital signal processing, and software of the HFA are described. In "Initial results" section, some initial results obtained during the period from January to July, 2017, are reported. In "Conclusion" section, a conclusion regarding the HFA initial analysis results is presented.

Instruments

A block diagram of HFA is shown in Fig. 1. The HFA is a subcomponent of the PWE onboard the Arase spacecraft. Two electric field components, E_u and E_v, are detected by WPT sensors (WPT-S-U1, WPT-S-U2, WPT-S-V1, and WPT-S-V2), converted to voltage signals, and fed to the HFA via the WPT preamplifiers (WPT-PRE-U1, WPT-PRE-U2, WPT-S-V1, and WPT-S-V2) and the differential amplifier in WFC/OFA. In addition, one component of the magnetic field, B_γ, is detected by the MSC, converted to a voltage signal, and fed to the HFA via the MSC preamplifier (MSC-PRE). The directions of E_u and E_v are perpendicular to the spin axis of the spacecraft, which is within 15° toward the sun. The direction of B_γ is parallel to the spin axis of the spacecraft (Kasahara et al. 2018b). The HFA consists of two channels of the analog receiver circuit (HFA-A) and digital circuit (HFA-D), with two
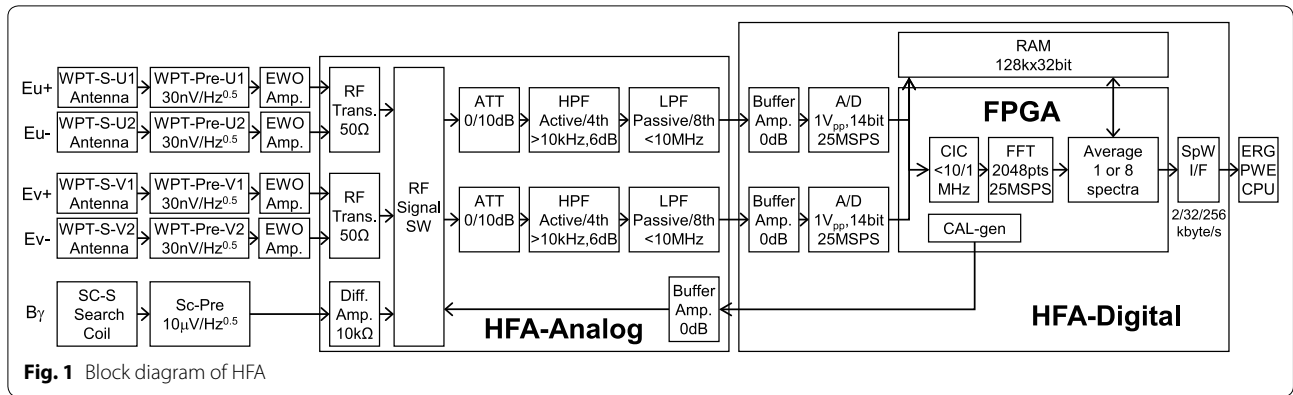
Kumamoto *et al. Earth, Planets and Space* (2018) 70:82

Page 3 of 14

Fig. 1 Block diagram of HFA

analog-to-digital converters (ADC) and one field programmable gate array (FPGA). In HFA-A, two signals from among the three possible inputs, E_u, E_v, and B_γ, are selected by radio frequency (RF) signal switch and fed to two channels of the receivers. The receivers consist of attenuators (0 or 10 dB), a high-pass filter (HPF), and a low-pass filter (LPF). The frequency range of E_u and E_v from WPT is from a few Hz to 10 MHz (Kasahara et al. 2018b), and the frequency range of B_γ from MSC is from a few Hz to 100 kHz (Ozaki et al. 2018). The passband of the receiver is from 10 kHz to 10 MHz. The analog signals are sampled by ADC with a 16-bit resolution in HFA-D with a sampling rate of 25 MHz. The spectra are obtained from the sampled digital waveform data in two signal processing modes. In 10 MHz mode, fast Fourier transform (FFT) is directly applied to the 2048 points of the digital waveform data. The spectrum below 12.5 MHz with 1024 frequency steps can be obtained. The frequency resolution is 12 kHz. In 1 MHz mode, a cascade integrator-comb (CIC) filter with a passband below 1 MHz and decimation is applied to the signal from ADC, which is converted to waveform data at 2.5 MSPS. FFT is applied to the 2048 points of the 2.5 MSPS waveform. The spectrum below 1.25 MHz with 1024 frequency steps

can be obtained. The frequency resolution is 1.2 kHz. Averaging over one spin period (8 s) can be applied to the obtained power spectrum and cross spectrum, which is useful for noise reduction.

The digital data of the spectrum are sent to a central processing unit (CPU) board in the PWE via the Spacewire interface and edited into mission data packets to be saved to the data recorder or sent via telemetry at the allowed rate. Two independent CPU boards (CPU#8 and CPU#9) are installed in the PWE, and CPU#8 is used for the HFA onboard data processing. Under nominal operation, three operation modes, EE, EB, and PP modes, are selected depending on the spacecraft location (Table 1). The EE mode is used around the apogee of the spacecraft orbit. In EE mode, E_u and E_v are selected by input signal switch, and power spectra of the electric fields, $\left\langle \left| \tilde{E}_u \right|^2 \right\rangle$ and $\left\langle \left| \tilde{E}_v \right|^2 \right\rangle$ (EE-UV mode), or the left- and right-handed electric fields, $\left\langle \left| \tilde{E}_L \right|^2 \right\rangle$ and $\left\langle \left| \tilde{E}_R \right|^2 \right\rangle$ (EE-LR mode), in a frequency range from 10 kHz to 10 MHz with 479 frequency steps, are obtained at 8-s intervals. $\tilde{E}_u$ and $\tilde{E}_v$ are the Fourier complex coefficients of E_u and E_v, respectively. $\tilde{E}_L$, and $\tilde{E}_R$ are given by

Table 1 Operation modes of HFA

Mode	Region	Input	Output	Frequency range	Steps	Interval (s)
EE-UV	Apogee	E_u, E_v	$<|E_u|^2>$	10 kHz–10 MHz	479	8
			$<|E_u|^2>$	10 kHz–10 MHz	479	8
EE-LR	Apogee	E_u, E_v	$<|E_L|^2>$	10 kHz–10 MHz	479	8
			$<|E_R|^2>$	10 kHz–10 MHz	479	8
EB	Perigee	E_v, B_γ	$<|E_v|^2>$	10 kHz–10 MHz	479	8
			$<|B_\gamma|^2>$	10 kHz–100 kHz	160	8
			$<E_v^* B_\gamma>$	10 kHz–100 kHz	160	8
PP-1	Plasmapause	E_u, E_v	$<|E_u|^2>+<|E_v|^2>$	10 kHz–400 kHz	200	1
PP-2	Plasmapause	E_u, E_v	$<|E_u|^2>+<|E_v|^2>$	100 kHz–1 MHz	200	1

Kumamoto *et al. Earth, Planets and Space* (2018) 70:82

Page 4 of 14

$$\left|\tilde{E}_L\right|^2 = \left|\tilde{E}_u + \tilde{E}_v \exp\left[-(\pi/2)i\right]\right|^2 \Big/ 2$$

$$= \left(\left|\tilde{E}_u\right|^2 + \left|\tilde{E}_u\right|^2\right)\Big/2 - \mathrm{Im}\,\tilde{E}_u\tilde{E}_v^* \tag{1}$$

$$\left|\tilde{E}_R\right|^2 = \left|\tilde{E}_u + \tilde{E}_v \exp\left[+(\pi/2)i\right]\right|^2 \Big/ 2$$

$$= \left(\left|\tilde{E}_u\right|^2 + \left|\tilde{E}_v\right|^2\right)\Big/2 + \mathrm{Im}\,\tilde{E}_u\tilde{E}_v^*, \tag{2}$$

where * indicates a complex conjugate and Im indicates an imaginary part. $\langle\ \rangle$ denotes the ensemble average of eight raw spectra obtained during one spin period. A frequency table of downlinked spectrum data is shown in Table 2. The downlinked spectrum data below 1 MHz and above 1 MHz are generated from 2.5 and 25 MSPS raw spectrum data, respectively. In order to reduce the data output rate, averaging among the intensities of raw spectra at neighboring frequency steps is also performed. The EB mode is used around the perigee, where the electron cyclotron frequency is higher than 20 kHz and the magnetic field component of the chorus emissions cannot be measured by WFC/OFA. In EB mode, E_v and B_γ are selected by input signal switch, and power spectrum of electric field $\left\langle\left|\tilde{E}_v\right|^2\right\rangle$ in a frequency range from 10 kHz to 10 MHz with 479 frequency steps, power spectrum of the magnetic field $\left\langle\left|\tilde{B}_\gamma\right|^2\right\rangle$ in a frequency range from 10 to 100 kHz with 160 frequency steps, and cross spectrum $\left\langle E_v B_\gamma^*\right\rangle$ in a frequency range from 10 to 100 kHz with 160 frequency steps are obtained at 8-s intervals. The PP mode is used around the plasmapause. In PP mode, E_u and E_v are selected by input signal switch, and power spectra of the electric fields $\left\langle\left|\tilde{E}_u\right|^2 + \left|\tilde{E}_v\right|^2\right\rangle$ in a frequency range from 10 to 400 kHz (PP-1 mode) or 100 kHz to 1 MHz (PP-2 mode) with 200 frequency steps

Table 2 Frequency table of downlinked spectrum data

Step	Frequency (MHz)	Bandwidth (kHz)
0–129	0.0024–0.1599	1.2
130–179	0.1624–0.2820	2.4
180–229	0.2856–0.5249	4.9
230–279	0.5322–1.0107	9.8
280–328	1.0132–1.5991	12.2
329–378	1.6235–2.8198	24.4
379–428	2.8564–5.2490	48.8
429–478	5.3223–10.1074	97.7

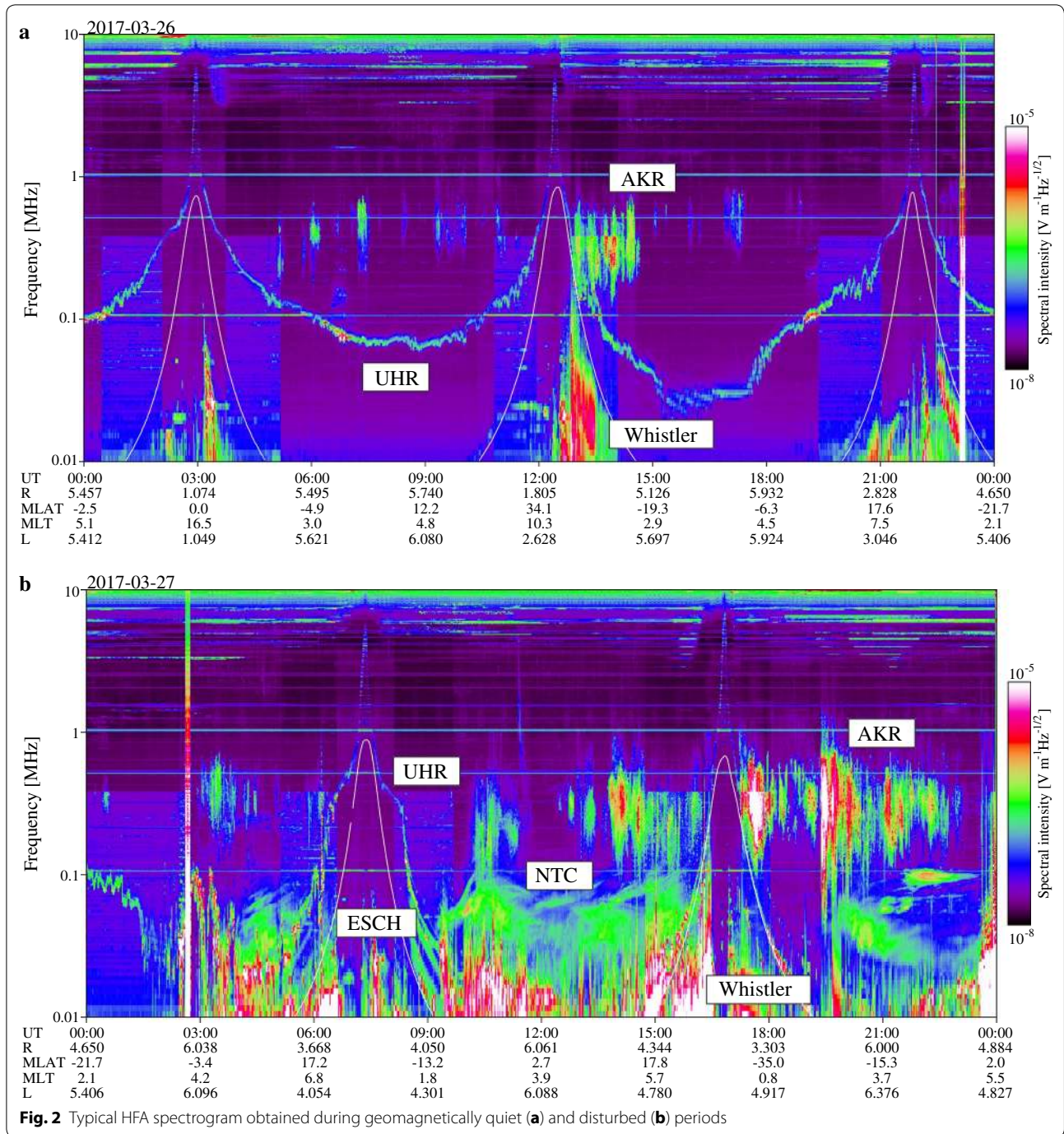are obtained at 1-s intervals in order to obtain high-resolution data of plasmapause structures.

In addition to editing the mission data packets, onboard software for the HFA is required to perform onboard automatic determination of UHR frequency using the HFA spectrogram. The determined UHR frequency is provided to S-WPIA at an interval of 1 s for onboard determination of the expected velocity of the resonant electrons with observed chorus emissions.

Initial results
Radio and plasma waves during geomagnetically quiet and disturbed periods
Typical spectrograms of radio and plasma waves obtained by HFA during geomagnetically quiet period (March 26, 2017; $0 \le \mathrm{Kp} \le 2$) and disturbed periods (March 27, 2017; $2 \le \mathrm{Kp} \le 6$) are shown in Fig. 2a, b, respectively. In both spectrograms, UHR waves, auroral kilometric radiation (AKR), and whistler-mode waves were observed. During the disturbed period, we find not only more intense AKR and whistler-mode waves but also electrostatic cyclotron harmonic (ESCH) waves and a nonthermal terrestrial continuum (NTC) (Brown 1973; Gurnett and Shaw 1973; Gurnett 1975). An expanded spectrogram of the ESCH waves is shown in Fig. 3. The ESCH emissions are found between the harmonics of electron cyclotron frequencies. The appearance and enhancement of radio and plasma waves such as UHR, ESCH, and NTC waves in a frequency range covered by the HFA in geomagnetically disturbed conditions suggest that there are energetic electrons that may be a free energy source of the plasma waves in the storm-time magnetosphere. It is therefore important to perform a detailed comparison between HFA data and the energetic electron data obtained by Arase/LEP-e (Low-Energy Particle Experiments-Electron Analyzer) (Kazama et al. 2017) and Arase/MEP-e (Medium-Energy Particle Experiments-Electron Analyzer) (Kasahara et al. 2018a). An example of the spectrograms obtained in PP-1 and EB modes is shown in Fig. 4. The AC electric field ($|E_u|^2 + |E_v|^2$ in PP-1 mode before 05:00 UT and $|E_v|^2$ in EB mode after 05:00 UT) is indicated in Fig. 4a. The AC magnetic field ($|B_\gamma|^2$ in EB mode) is indicated in Fig. 4b. Spectra of the electric and magnetic fields of the whistler-mode wave above 10 kHz were observed by the HFA in EB mode. Example of the high-time resolution spectrogram obtained in PP-1 mode is shown in Fig. 5. The spacecraft passed through the plasmapause from 07:42 to 07:51 UT. We observe fluctuations in the UHR frequency at the plasmapause and fine structures in AKR.

After confirming that the gains of E_u and E_v are the same in the EE-UV mode operation performed in initial check phase, we started the operation in EE-LR mode, in which the left- and right-handed

Kumamoto *et al. Earth, Planets and Space* (2018) 70:82

Page 5 of 14

Fig. 2 Typical HFA spectrogram obtained during geomagnetically quiet (**a**) and disturbed (**b**) periods

electric fields, $\left\langle \left| \tilde{E}_L \right|^2 \right\rangle$ and $\left\langle \left| \tilde{E}_R \right|^2 \right\rangle$, are obtained. A typical example of the spectrogram obtained in test operations of EE-LR mode on June 10, 2017, is shown in Fig. 6. The total intensity of left- and right-handed components $\left\langle \left| \tilde{E}_R \right|^2 \right\rangle + \left\langle \left| \tilde{E}_L \right|^2 \right\rangle$ and the axial ratio

$\left(\left\langle \left| \tilde{E}_R \right|^2 \right\rangle - \left\langle \left| \tilde{E}_L \right|^2 \right\rangle \right) \Big/ \left(\left\langle \left| \tilde{E}_R \right|^2 \right\rangle + \left\langle \left| \tilde{E}_L \right|^2 \right\rangle \right)$ of the radio and plasma waves are indicated in Fig. 6a, b, respectively. Since the polarization in the HFA observation is defined with respect to the anti-sunward direction, and the magnetic field is in the sunward direction in the northern hemisphere on the night side, the positive axial ratio (red) indicates left-hand polarization
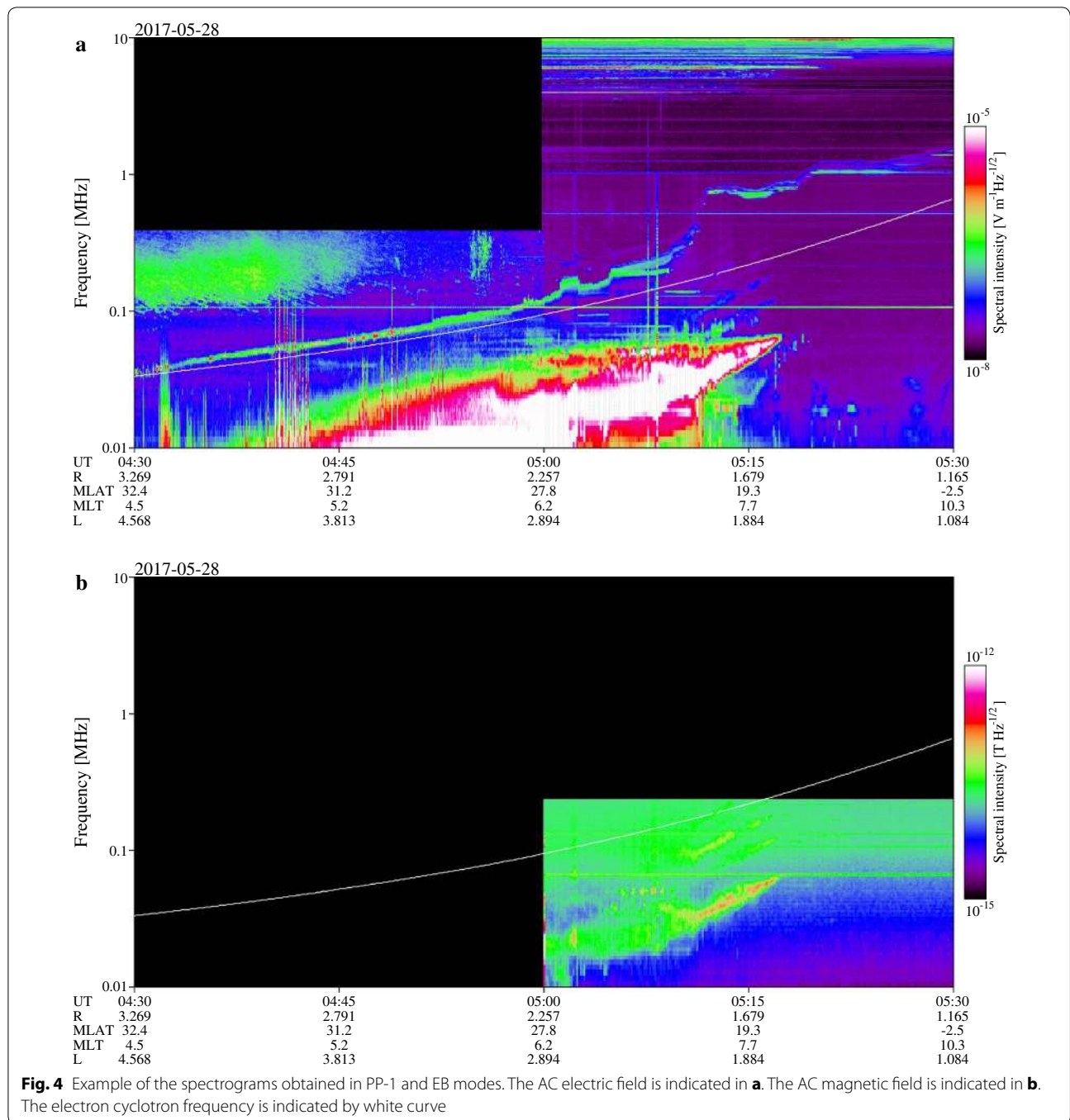
Kumamoto *et al. Earth, Planets and Space* (2018) 70:82

Page 6 of 14
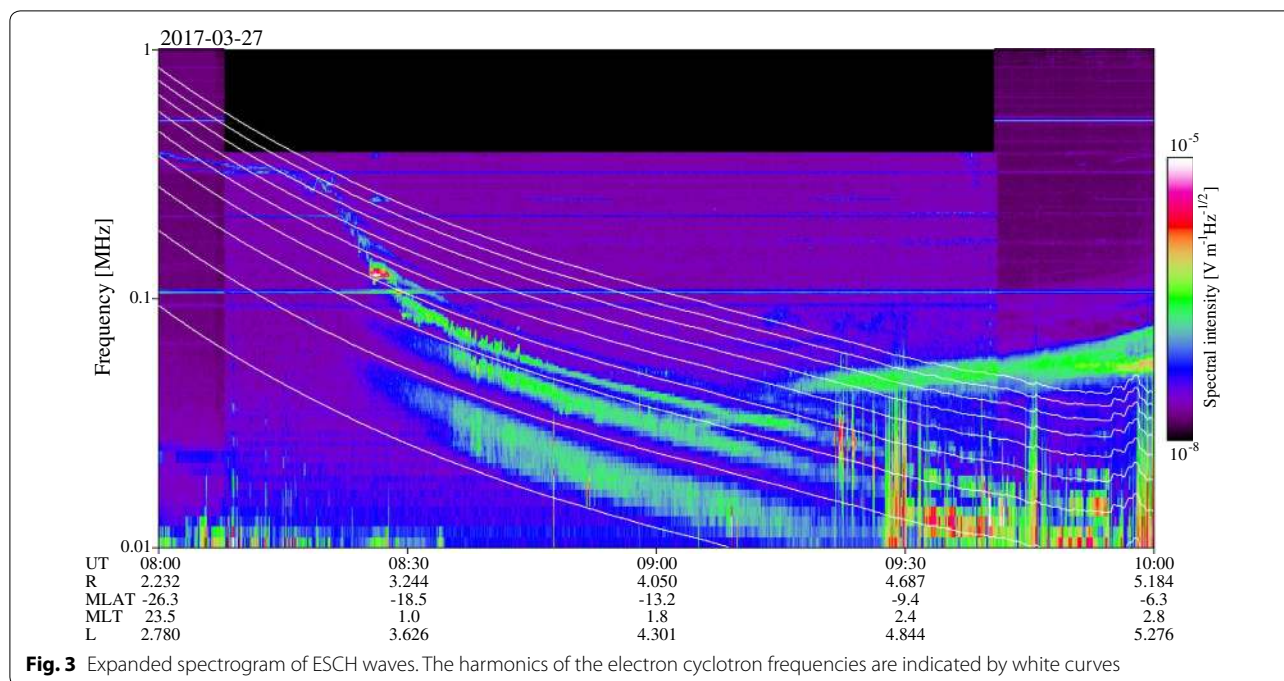
Fig. 3 Expanded spectrogram of ESCH waves. The harmonics of the electron cyclotron frequencies are indicated by white curves

with respect to the magnetic field; a negative axial ratio (blue) indicates right-hand polarization with respect to the magnetic field. AKR in a frequency range from 100 to 500 kHz is found in the spectrograms. There are both polarized components below 300 kHz and right-handed component only above the 300 kHz. In addition, although some of left-handed components (red) below 300 kHz are masked by intense right-handed components (blue), left-handed components (red) below 300 kHz always accompany right-handed components (blue) with similar spectral structures above 300 kHz. In this observation, the spacecraft is around a geocentric distance of 5 R_E and a geomagnetic latitude of $+30°$, and AKR from the southern polar region cannot be observed due to shielding by the plasmasphere. Therefore, the AKR is considered to be from two different sources in the northern polar regions. One is the typical R-X mode AKR below 300 kHz, and the other is the fundamental L-O mode AKR below 300 kHz, with the second-harmonic component in R-X mode as reported by several previous studies (Benson 1982; Mellott et al. 1986). They are suggested to be generated depending on plasma density in AKR sources; when $f_\mathrm{pe}/f_\mathrm{ce}$ is less than 0.3, a high growth rate in R-X mode is expected. When $f_\mathrm{pe}/f_\mathrm{ce}$ is as large as 0.3, the growth rate in the fundamental L-O mode and second-harmonic R-X mode can be higher than that in the fundamental R-X mode (Wu and Qiu 1983; Melrose et al. 1984). The AKR from two sources at different locations is considered to be observed simultaneously probably due to the effects

of mode filtering around the plasmasphere, as discussed by Hashimoto (1984). We also checked the survey plot of Cluster/WBD (Gurnett et al. 1997) provided via http://www-pw.physics.uiowa.edu/cluster/ and confirmed that the spectra of intense (probably right-handed) AKR observed by Cluster in the southern hemisphere are quite different from the spectra of left-handed AKR observed by Arase in the northern hemisphere. This also suggests that the left-handed AKR observed by Arase in the northern hemisphere is not from the R-X mode AKR sources in the southern hemisphere. The start of EE-LR mode observation will bring us useful datasets for discussions on the plasma conditions, generation mechanisms at the AKR sources, and AKR propagation from the sources in the both northern and southern polar regions.

Datasets obtained in EE-LR mode will also be useful with regard to discussions on not only AKR but also kilometric continuum (KC). Since KC is observed as L-O mode waves in most cases, KC is considered to be generated by the linear mode conversion processes in plasma density gradients around the plasmapause. On the other hand, Kalaee and Katoh (2016) reported that R-X mode KC are also observed by the Akebono satellite, suggesting that R-X mode waves can be generated by nonlinear interactions between Z-mode waves and energetic electrons based on simulations. Further discussion will be enabled by HFA EE-LR mode data and energetic electron data around the plasmapause obtained by Arase/LEP-e (Kazama et al. 2017) and MEP-e (Kasahara et al. 2018a).

Kumamoto *et al. Earth, Planets and Space* (2018) 70:82

Page 7 of 14

Fig. 4 Example of the spectrograms obtained in PP-1 and EB modes. The AC electric field is indicated in **a**. The AC magnetic field is indicated in **b**. The electron cyclotron frequency is indicated by white curve

UHR frequency identification for derivation of electron number density

Electron number density is a key parameter in the discussion of structure and evolution of the plasmasphere, as well as the resonance conditions of electrons with plasma waves in the wave–particle interaction phenomena. Because UHR frequency, the upper frequency of the UHR waves, depends on the plasma frequency f_{pe} and electron cyclotron frequency f_{ce}, and because f_{ce} can be derived from magnetic field intensity measured by the Arase/Magnetic Field Experiment (MGF) (Matsuoka et al. 2018), we can thus derive f_{pe} and electron number density. While the derivation of the electron number density from UHR frequency and f_{ce} is quite easy, it is not easy to obtain the UHR frequency from the HFA spectrogram data. The first difficulty is that the number

Kumamoto *et al. Earth, Planets and Space* (2018) 70:82

Page 8 of 14
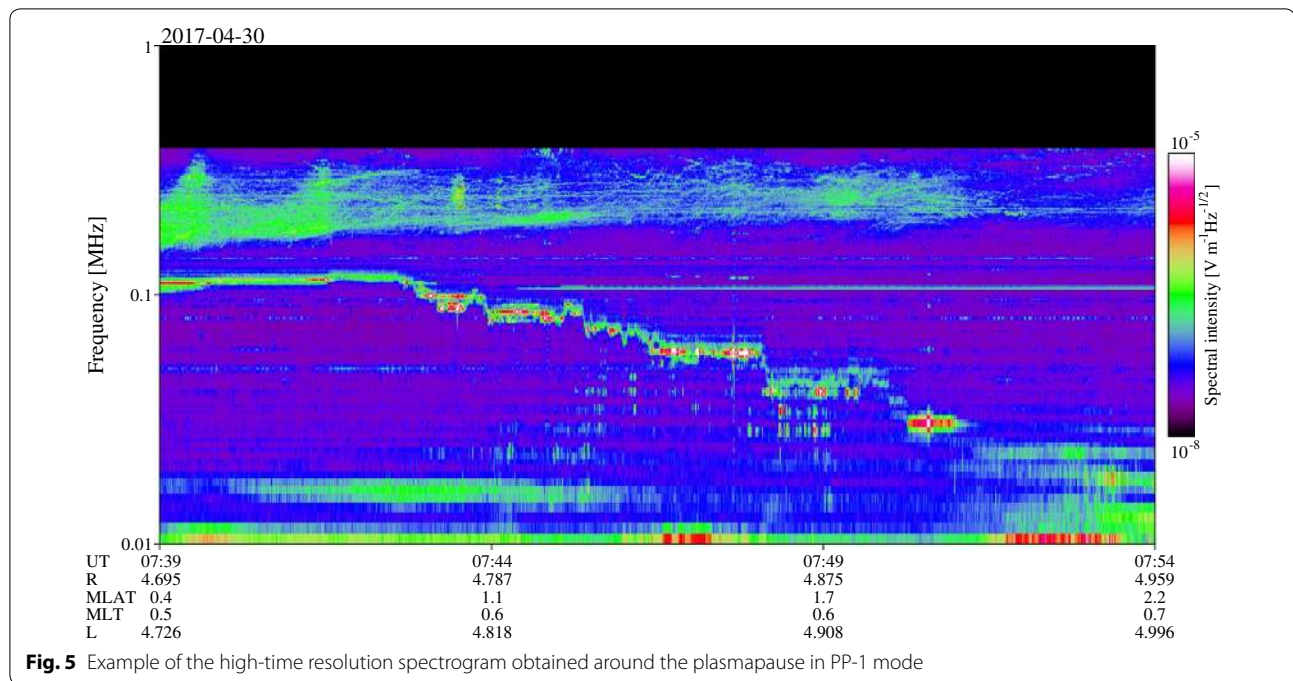
Fig. 5 Example of the high-time resolution spectrogram obtained around the plasmapause in PP-1 mode

of HFA spectrograms is too large for a manual trace of UHR emissions in the spectrogram. We usually obtain about six spectrograms between the apogee and perigee per day. If we use 10 min on average for a manual trace of UHR frequency in each spectrogram, 30 h of work is required for one month of HFA spectrogram data. This is not impossible but very difficult to execute with constant quality by a human operator. The second difficulty is that there are cases in which UHR emissions are difficult to identify. Under geomagnetically quiet conditions, as shown in Fig. 2a, UHR emissions are easy to identify. However, under disturbed conditions, as shown in Fig. 2b, UHR emissions become difficult to identify, especially outside of the plasmasphere. Therefore, trials for full automatic identification of the UHR waves by computer will require a significant amount of time and effort, and this does not seem to be a good approach for obtaining the electron number density as early as possible.

In this study, we chose an approach with semiautomatic identification of UHR frequency by the computer and a human operator. First, we applied an algorithm for identification of the UHR frequency to the HFA spectrogram data. The algorithm was developed not to identify UHR frequency in all cases but to identify it in easy cases. Then, a human operator checked the identifications made by the computer and corrected them if needed. A similar approach was also used by Kurth et al. (2015) to identify UHR frequency in spectrograms obtained by the Van Allen Probe. They also mentioned that inspections and corrections by a human operator were necessary.

They used an algorithm called AURA (automated upper hybrid resonance detection algorithm), which identifies the UHR frequency at the peak of the spectrum weighted by a Gaussian function whose peak is at the previously identified UHR frequency. Although the algorithm is quite simple, and seems sufficiently effective, we used another step-by-step algorithm so that we could arrange multiple criteria and parameters manually to improve UHR identification.

In the step-by-step algorithm used in this study, candidates of UHR frequency in the spectrogram are selected by checking for several conditions. As a typical example, the result of UHR identification in the HFA spectrogram obtained on March 26, 2017, is shown in Fig. 7. In Step 1, we prepared the spectrogram data with 479 frequency steps at an interval of 1 min (Fig. 7a). In Step 2, the emissions with an intensity greater than 4×10^{-8} Vm^{-1}Hz$^{-1/2}$ (10 dB above the noise level averaged over one spin period) in a frequency range above the electron cyclotron frequency were selected out as candidates of UHR frequency (Fig. 7b). In Step 3, known artificial noises were removed (Fig. 7c). In Step 4, a median filter was applied to windows with a size of five frequency steps (Fig. 7d). In Step 5, the emissions with a bandwidth larger than 200 kHz were removed (Fig. 7e). In Step 6, the upper limit frequency of the emissions was selected (Fig. 7f).

In case of the spectrogram obtained on March 26, 2017, under geomagnetically quiet conditions, the UHR frequency could be identified well by the algorithm mentioned above, as shown in Fig. 8a. However, in case of
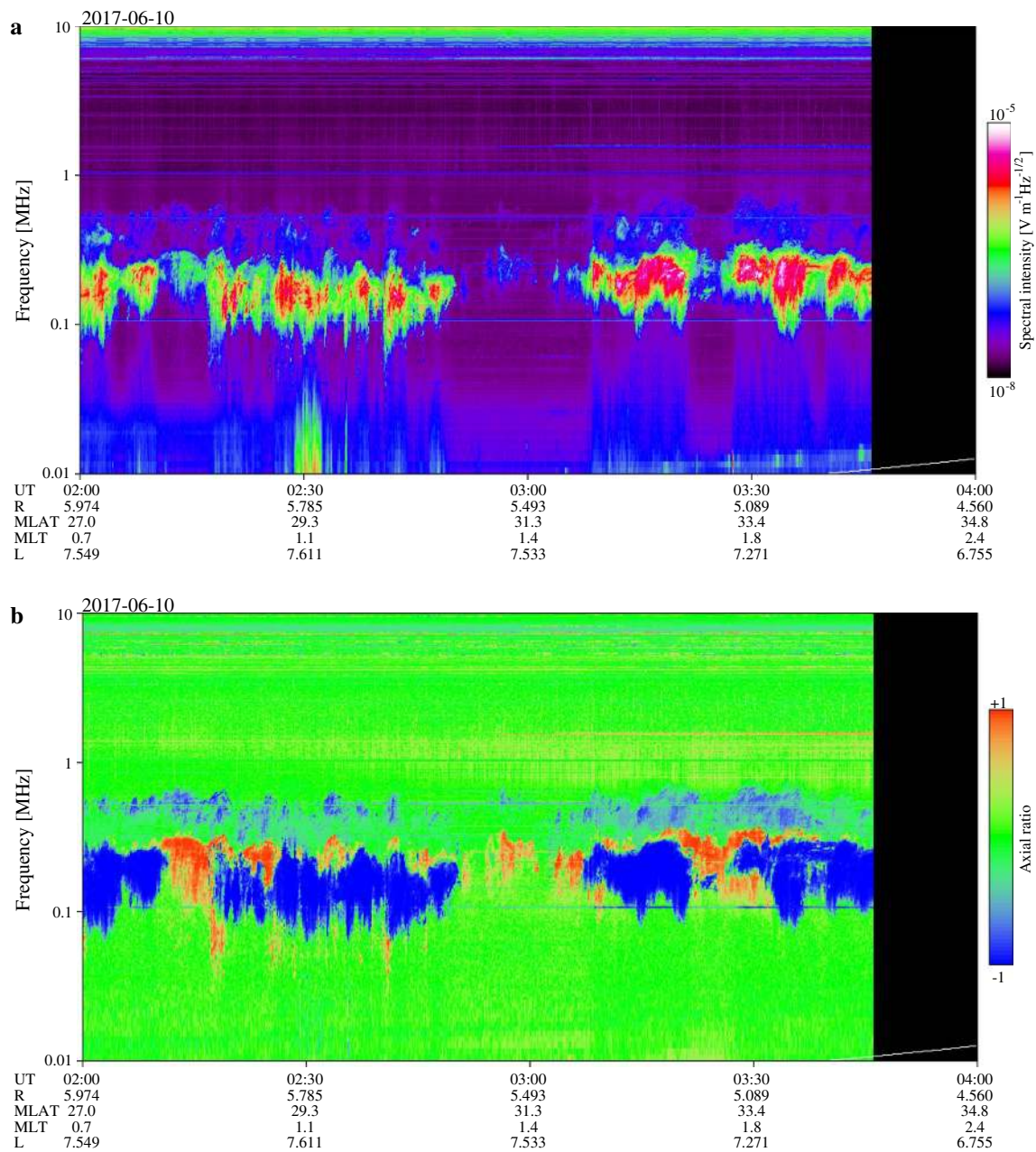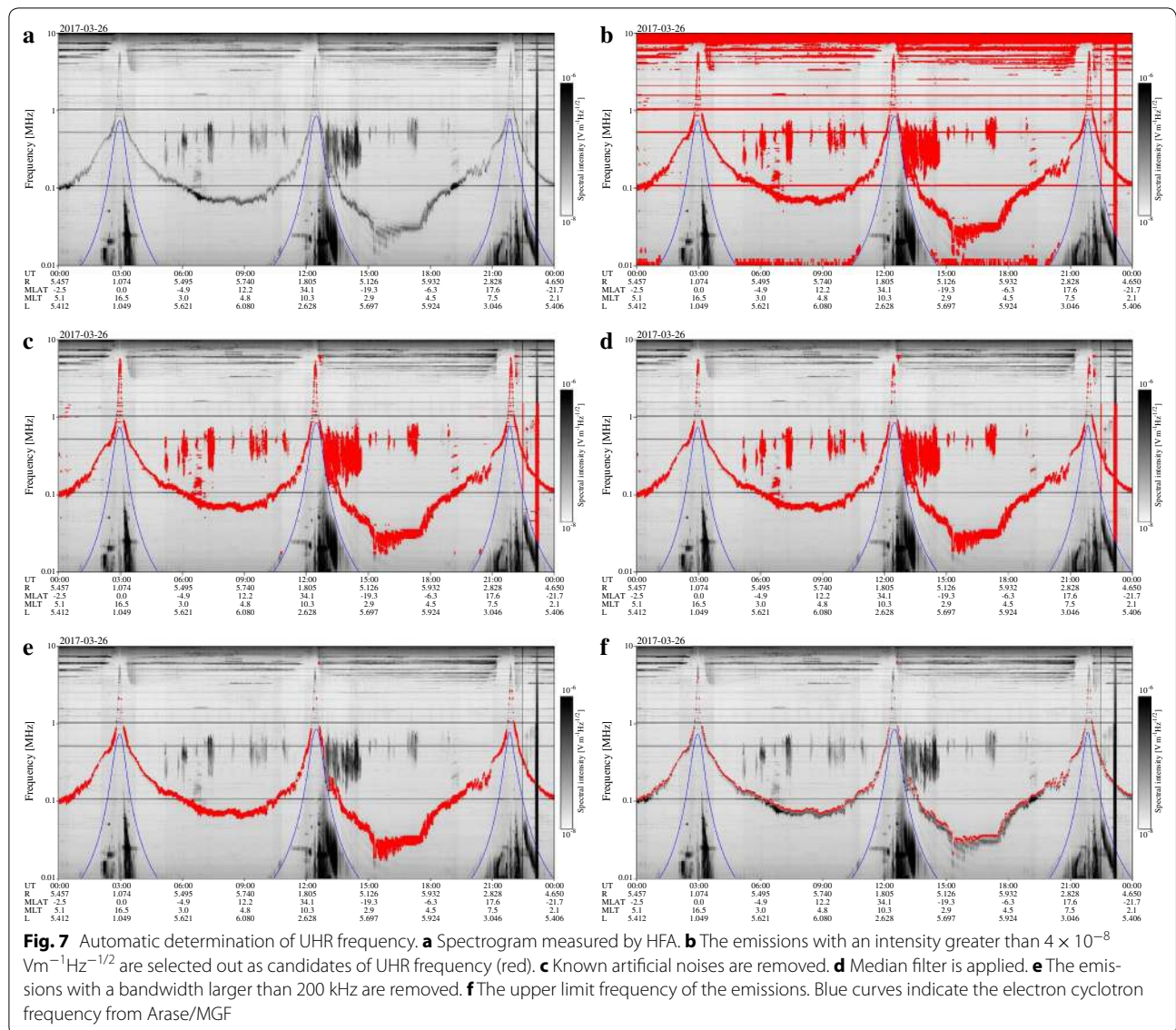
Kumamoto *et al. Earth, Planets and Space* (2018) 70:82

Page 9 of 14

Fig. 6 Intensity (**a**) and axial ratio (**b**) of AKR measured on June 10, 2017. Right- and left-handed radio waves with respect to the background magnetic field are indicated in blue and red, respectively

spectrogram obtained on March 27, 2017, under geomagnetically disturbed conditions, the UHR frequency could not be identified well by the same algorithm. Therefore, we performed manual corrections in cases such as this. As shown during the periods of 5:00–7:00, 8:00–9:00, 15:00–16:00, and 18:00–19:00 UT in Fig. 8b, incorrect traces by the computer were retraced by the human operator. As shown during the periods of 13:00–15:00, and

19:00–22:00 UT in Fig. 8c, UHR identification was often difficult, even by the human operator. In such cases, the human operator only performed removal of the incorrect traces by the computer.

The semiautomatic UHR identification mentioned above was applied to the HFA spectrogram datasets obtained from January to July, 2017. The electron number densities derived from the UHR frequency from the

Kumamoto *et al. Earth, Planets and Space* (2018) 70:82

Page 10 of 14

Fig. 7 Automatic determination of UHR frequency. **a** Spectrogram measured by HFA. **b** The emissions with an intensity greater than 4×10^{-8} $Vm^{-1}Hz^{-1/2}$ are selected out as candidates of UHR frequency (red). **c** Known artificial noises are removed. **d** Median filter is applied. **e** The emissions with a bandwidth larger than 200 kHz are removed. **f** The upper limit frequency of the emissions. Blue curves indicate the electron cyclotron frequency from Arase/MGF

HFA and electron cyclotron frequency from Arase/MGF as a function of *L* value are shown in Fig. 9. We find two distinct trends: One is with respect to the electron number density in the plasmasphere, and the other concerns that in the trough regions outside of the plasmapause, as reported by Sheeley et al. (2001) based on CRRES (The Combined Release and Radiation Effects Satellite) observations. While most profiles of the plasmaspheric electron number density are within 7 R_E, there are also some profiles extending to 8–8.5 R_E. The nearest trough is around 2.5–3 R_E, which seems to include the inner trough within the plasmapause. The dataset of electron number density inside and outside the plasmasphere during several months obtained by Arase will be useful for discussions of the evolution of the plasmasphere. Several

studies have suggested that some unusual electric fields appear in the storm-time inner magnetosphere, in addition to convection electric fields, as modeled by Maynard and Chen (1975). Oya (1997) suggested the effects of betatron electric fields on the plasmaspheric structures based on UHR observations by the Akebono satellite. Based on the statistical analyses of the electric field data obtained by the Akebono satellite, Nishimura et al. (2006) suggested that storm-time electric field components appear around $L = 3$. They are considered to evolve depending not simply on geomagnetic indices such as Kp, Dst, and AE, but also with respect to the phases of geomagnetic storms. Further investigation of the evolutions of plasmaspheric structures and the contributions of such storm-time electric fields on them will be
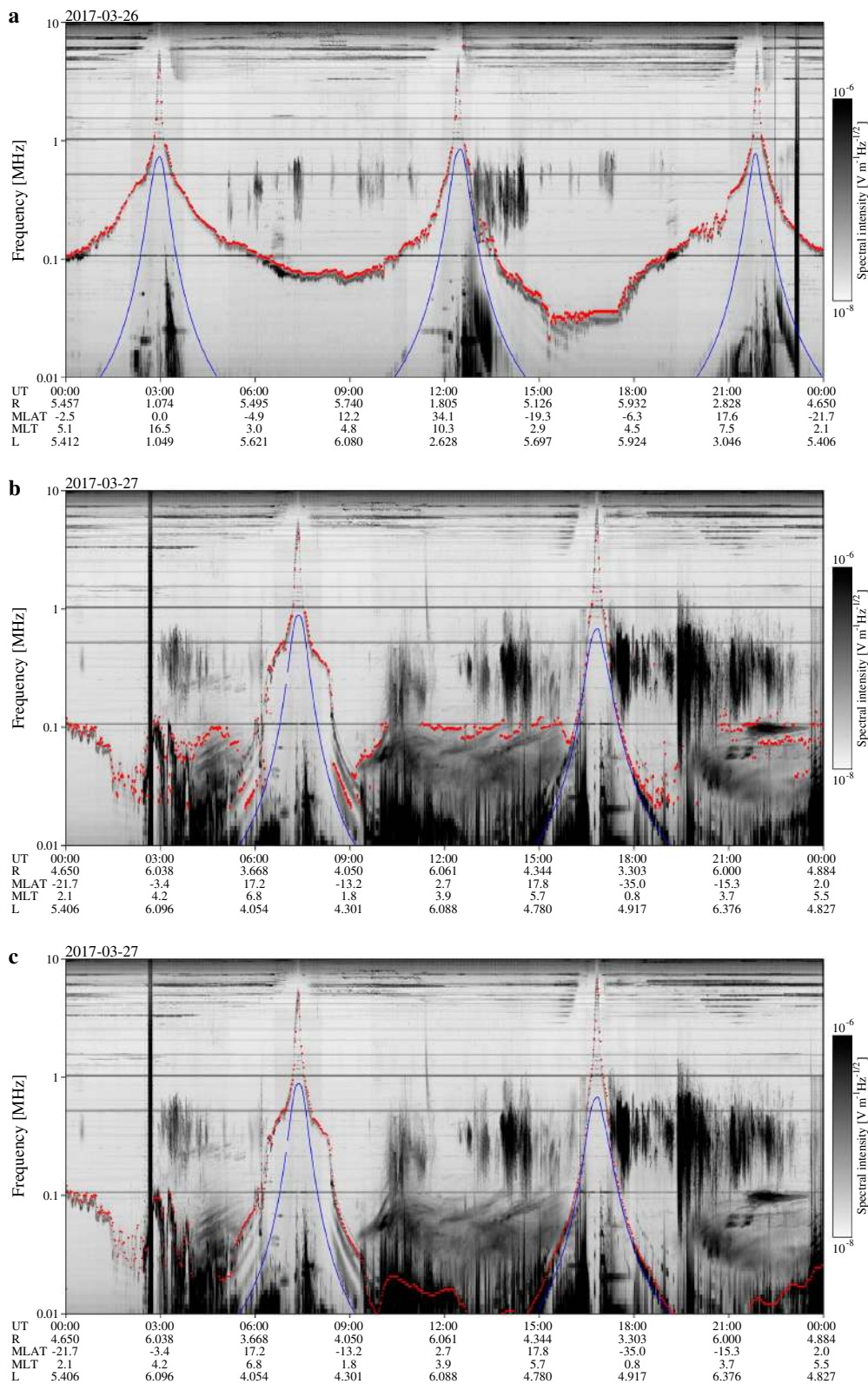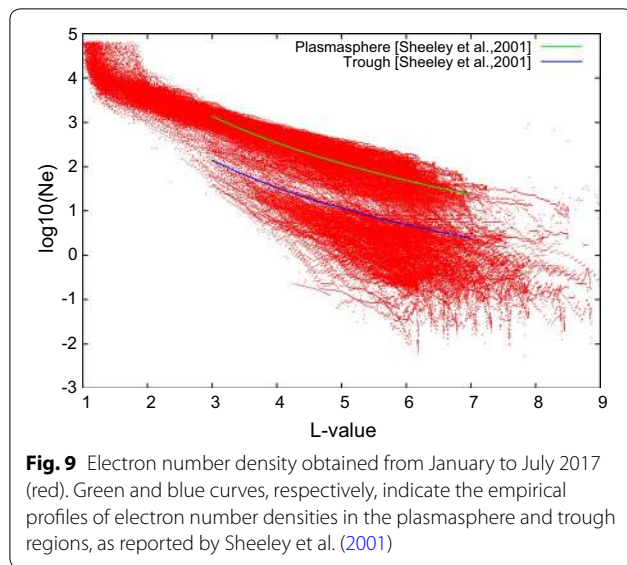
Kumamoto *et al. Earth, Planets and Space* (2018) 70:82

Page 11 of 14

Fig. 8 Comparisons of identified UHR frequency. **a** UHR frequency automatically determined under geomagnetically quiet conditions. **b** UHR frequency automatically determined under geomagnetically disturbed conditions. **c** UHR frequency after the manual correction of that in **b**

Kumamoto *et al. Earth, Planets and Space* (2018) 70:82

Page 12 of 14

Fig. 9 Electron number density obtained from January to July 2017 (red). Green and blue curves, respectively, indicate the empirical profiles of electron number densities in the plasmasphere and trough regions, as reported by Sheeley et al. (2001)

possible with electron number density datasets obtained from HFA observations. Since the perigee of the Arase is 460 km, the dataset will be useful for studies of the topside ionosphere.

Conclusion

HFA is designed to (1) determine the electron number density around the spacecraft from the observation of UHR waves, (2) measure the electromagnetic field component of the whistler-mode chorus in a frequency range above 20 kHz up to 100 kHz, and (3) observe radio and plasma waves excited by wave–particle interactions and mode conversion processes in a storm-time magnetosphere. AC electric fields E_u and E_v detected by WPT-S and the AC magnetic field B_γ detected by MSC are fed to the HFA. By applying analog and digital signal processing in the HFA, the spectrograms of two electric fields (EE mode) or one electric filed and one magnetic field (EB mode) in a frequency range from 10 kHz to 10 MHz are obtained at an interval of 8 s. For the observation of plasmapause, the HFA can also be operated in PP mode, in which spectrograms of one electric field component below 1 MHz are obtained at an interval of 1 s. During the initial HFA operations from January to July, 2017, the following results were obtained: (1) UHR wave, AKR, whistler-mode chorus, ESCH wave, and NTC radiation could be observed by HFA. Their intensity depended upon geomagnetic conditions. (2) During the test operation in EE-LR mode on June 10, 2017, the fundamental R-X and L-O mode AKR and the second-harmonic R-X mode AKR from different sources in the northern polar region were observed. (3) A semiautomatic UHR frequency identification by the computer and a human

operator was applied to the HFA spectrograms obtained from January to July, 2017. In the identification by the computer, we used an algorithm for narrowing down the candidates of UHR frequency that included an intensity check, removal of the known noises, median filter, and bandwidth check. After identification by the computer, the identified UHR frequency was checked and corrected, if needed, by the human operator. From the determined UHR frequency, electron number density in the plasmasphere and trough regions outside of the plasmapause from January to July, 2017, was derived, which were similar with those reported in the previous studies (Sheeley et al. 2001).

The algorithm and parameters used in the automatic part of UHR identification will be used in the HFA operation for providing electron number density to S-WPIA, which is being tested. Electron number density obtained from semiautomatic UHR identification will be essential for analyses of wave–particle interactions between the whistler-mode chorus and energetic electrons, which is a focus of the Arase mission. In addition, the dataset of electron number density will be useful for investigating storm-time evolutions of the plasmasphere and topside ionosphere.

Author details

[1] Tohoku University, 6-3, Aoba, Aramaki, Aoba, Sendai 980-8578, Japan. [2] Kanazawa University, Kakuma-machi, Kanazawa 920-1192, Japan. [3] Kyoto University, Gokasho, Uji 611-0011, Japan. [4] Toyama Prefectural University, 5180, Kurokawa, Imizu 939-0398, Japan. [5] Nagoya University, Furou-cho, Chikusa, Nagoya 464-8601, Japan. [6] ISAS, JAXA, 3-1-1, Yoshinodai, Chuo, Sagamihara 252-5210, Japan.

Kumamoto *et al. Earth, Planets and Space* (2018) 70:82

Page 13 of 14

Competing interests
The authors declare that they have no competing interests.

Availability of data and materials
The HFA data will be distributed from the ERG Science Center operated by ISAS/JAXA and ISEE/Nagoya University.

Consent for publication
Not applicable.

Ethics approval and consent to participate
Not applicable.

Publisher's Note
Springer Nature remains neutral with regard to jurisdictional claims in published maps and institutional affiliations.

References

Benson RF (1982) Harmonic auroral kilometric radiation of natural origin. Geophys Res Lett 9:1120–1123. https://doi.org/10.1029/GL009i009p01120

Brown LW (1973) The galactic radio spectrum between 130 kHz and 2600 kHz. Astrophys J 180:359–370. https://doi.org/10.1086/151968

Gurnett DA (1975) The Earth as a radio source: the nonthermal continuum. J Geophys Res 80:2751–2763. https://doi.org/10.1029/JA080i019p02751

Gurnett DA, Shaw RR (1973) Electromagnetic radiation trapped in the magnetosphere above the plasma frequency. J Geophys Res 78:8136–8149. https://doi.org/10.1029/JA078i034p08136

Gurnett DA, Huff RL, Kirchner DL (1997) The wide-band plasma wave investigation. Space Sci Rev 79:195–208. https://doi.org/10.1023/A:1004966823678

Hashimoto K (1984) A reconciliation of propagation modes of auroral kilometric radiation. J Geophys Res 89:7459–7466. https://doi.org/10.1029/JA089iA09p07459

Hikishima M et al (2018) Data processing in the software-type wave-particle interaction analyzer on board the Arase satellite. Earth Planets Space. https://doi.org/10.1186/s40623-018-0856-y

Kalaee MJ, Katoh Y (2016) A simulation study of RX-mode waves generation in the equatorial plasmasphere. Iranian J. Geophys. 9(5):1–10

Kasaba Y, Ishisaka I, Kasahara Y, Imachi T, Yagitani S, Kojima H, Matsuda S, Shoji M, Kurita S, Hori T, Shinbori A, Teramoto M, Miyoshi Y, Nakagawa T, Takahashi N, Nishimura Y, Matsuoka A, Kumamoto A, Tsuchiya F, Nomura R (2017) Wire probe antenna (WPT) and electric field detector (EFD) of plasma wave experiment (PWE) aboard Arase: specifications and initial evaluation results. Earth Planets Space. https://doi.org/10.1186/s40623-017-0760-x

Kasahara S, Yokota S, Mitani T, Asamura K, Hirahara M, Shibano Y, Takashima T (2018a) Medium-Energy Particle Experiments—electron analyzer (MEP-e) for the Exploration of Energization and Radiation in Geospace (ERG) mission. Earth Planets Space. https://doi.org/10.1186/s40623-018-0847-z

Kasahara Y, Kasaba Y, Kojima H, Yagitani S, Ishisaka K, Kumamoto A, Tsuchiya F, Ozaki M, Matsuda S, Imachi T, Miyoshi Y, Hikishima M, Katoh Y, Ota M, Shoji M, Matsuoka A, Shinohara I (2018b) The Plasma Wave Experiment (PWE) on board the Arase (ERG) satellite. Earth Planets Space. https://doi.org/10.1186/s40623-018-0842-4

Katoh Y, Kojima H, Hikishima M, Takashima T, Asamura K, Miyoshi Y, Kasahara Y, Kasahara S, Mitani T, Higashio N, Matsuoka A, Ozaki M, Yagitani S, Yokota S, Matsuda S, Kitahara M, Shinohara I (2018) Software-type wave-particle interaction analyzer on board the Arase satellite. Earth Planets Space 70:4. https://doi.org/10.1186/s40623-017-0771-7

Kazama Y, Wang B-J, Wang S-Yu, Ho PTP, Tam SWY, Chang TF, Chiang CY, Asamura K (2017) Low-energy particle experiments—electron analyzer (LEPe) onboard the Arase spacecraft. Earth Planet Space. https://doi.org/10.1186/s40623-017-0748-6

Kurth WS, DePascuale S, Faden JB, Kletzing CA, Hospodarsky GB, Thaller S, Wygant JR (2015) Electron densities inferred from plasma wave spectra obtained by the Waves instrument on Van Allen Probes. J Geophys Res Space Phys 120:904–914. https://doi.org/10.1002/2014ja020857

Matsuda S, Kasahara Y, Kojima H, Kasaba Y, Yagitani S, Ozaki M, Imachi T, Ishisaka K, Kumamoto A, Tsuchiya F, Ota M, Kurita S, Miyoshi Y, Hikishima M, Matsuoka A, Shinohara I (2018) Onboard software of plasma wave experiment aboard Arase: instrument management and signal processing of waveform capture/onboard frequency analyzer. Earth Planets Space. https://doi.org/10.1186/s40623-018-0838-0

Matsuoka A, Teramoto M, Nomura R, Nosé M, Fujimoto A, Tanaka Y, Shinohara M, Nagatsuma T, Shiokawa K, Obana Y, Miyoshi Y, Mita M, Takashima T, Shinohara I (2018) The Arase (ERG) magnetic field investigation. Earth Planets Space. https://doi.org/10.1186/s40623-018-0800-1

Maynard NC, Chen AJ (1975) Isolated cold plasma regions: observations and their relation to possible production mechanisms. J Geophys Res 80:1009–1013. https://doi.org/10.1029/JA080i007p01009

Mellott MM, Huff RL, Gurnett DA (1986) DE-1 observations of harmonic auroral kilometric radiation. J Geophys Res 91:13:732–13,738. https://doi.org/10.1029/ja091ia12p13732

Melrose DB, Hewitt RG, Dulk GA (1984) Electron-cyclotron maser emission: relative growth and damping rates for different modes and harmonics. J Geophys Res 89:897–904. https://doi.org/10.1029/JA089iA02p00897

Miyoshi Y, Morioka A, Obara T, Misawa H, Nagai T, Kasahara Y (2003) Rebuilding process of the outer radiation belt during the 3 November 1993 magnetic storm: NOAA and Exos-D observations. J Geophys Res 108(A1):1004. https://doi.org/10.1029/2001JA007542

Miyoshi Y, Ono T, Takashima T, Asamura K, Hirahara M, Kasaba Y, Matsuoka A, Kojima H, Shiokawa K, Seki K, Seki K, Fujimoto M, Nagatsuma T, Cheng CZ, Kazama Y, Kasahara S, Mitani T, Matsumoto H, Higashio N, Kumamoto A, Yagitani S, Kasahara Y, Ishisaka K, Blomberg L, Fujimoto A, Katoh Y, Ebihara Y, Omura Y, Nosé M, Hori T, Miyashita Y, Tanaka Y-M, Segawa T (2012) The energization and radiation in geospace (ERG) project. In: Summers D, Mann IR, Baker DN, Schulz M (eds) Dynamics of the Earth's radiation belts and inner magnetosphere. Wiley, Hoboken, pp 103–116. https://doi.org/10.1029/2012gm001304

Nishimura Y, Shinbori A, Ono T, Iizima M, Kumamoto A (2006) Storm-time electric field distribution in the inner magnetosphere. Geophys Res Lett 33:L22102. https://doi.org/10.1029/2006GL027510

Ono T, Oya H, Morioka A, Kumamoto A, Kobayashi K, Obara T, Nakagawa T (1998) Plasma waves and sounder (PWS) experiment on-board the PLANET-B Mars orbiter. Earth Planets Space 50:213–222. https://doi.org/10.1186/BF03352106

Ono T, Kumamoto A, Yamaguchi Y, Yamaji A, Kobayashi T, Kasahara Y, Oya H (2008) Instrumentation and observation target of the Lunar Radar Sounder (LRS) experiment on-board the SELENE spacecraft. Earth Planets Space 60:321–332. https://doi.org/10.1186/BF03352797

Ono T, Kumamoto A, Kasahara Y, Yamaguchi Y, Yamaji A, Kobayashi T, Oshigami S, Nakagawa H, Goto Y, Hashimoto K, Omura Y, Imachi T, Matsumoto H, Oya H (2010) The Lunar Radar Sounder (LRS) Onboard the KAGUYA (SELENE) Spacecraft. Space Sci Rev 154:145–192. https://doi.org/10.1007/s11214-010-9673-8

Oya H (1997) Dynamical Variation of Plasmasphere Revealed by PWS Data onboard the Akebono (EXOS-D) Satellite. J Geomag Geoelectr 49:S159–S178. https://doi.org/10.5636/jgg.49.Supplement_S159

Oya H, Ono T, Kamada T (1981) Stimulation of plasma waves in the magnetosphere using satellite JIKIKEN (EXOS-B), Part-I: observation of plasma

Kumamoto *et al. Earth, Planets and Space* (2018) 70:82

Page 14 of 14

resonances. J Geomag Geoelectr 33:3–25. https://doi.org/10.5636/jgg.33.3

Oya H, Morioka A, Obara T (1985) Leaked AKR and terrestrial hectometric radiations discovered by the plasma wave and planetary plasma sounder experiments on board the Ohzora (EXOS-C) satellite—instrumentation and observation results of plasma wave phenomena. J Geomag Geoelectr 37:237–262. https://doi.org/10.5636/jgg.37.237

Oya H, Morioka A, Kobayashi K, Iizima M, Ono T, Miyaoka H, Okada T, Obara T (1990) Plasma wave observations and sounder experiments (PWS) on board Akebono (EXOS-D) satellite. J Geomag Geoelectr 42:411–442. https://doi.org/10.5636/jgg.42.411

Ozaki M, Yagitani S, Kasahara Y, Kojima H, Kasaba Y, Kumamoto A, Tsuchiya F, Matsuda S, Matsuoka A, Sasaki T, Yumoto T (2018) The magnetic search coil (MSC) of plasma wave experiment (PWE) aboard the Arase (ERG) satellite. Earth Planets Space. https://doi.org/10.1186/s40623-018-0837-1

Sheeley BW, Moldwin MB, Rassoul HK, Anderson RR (2001) An empirical plasmasphere and trough density model: CRRES observations. J Geophys Res 106(A11):25,631–25,641. https://doi.org/10.1029/2000ja000286

Wu CS, Qiu XM (1983) Emissions of second-harmonic auroral kilometric radiation. J Geophys Res 88:10,072–10,080. https://doi.org/10.1029/ja088ia12p10072